RSC Advances

ROYAL SOCIETY OF CHEMISTRY

www.rsc.org/advances

Controlled Synthesis of Peony-Shaped Photocatalyst Grains of $Ag_3PO_4/Zn_3(PO_4)_2$ by Coprecipitation and Recrystallization Technology

Ma Peiyan[a], Yu Yong[a],Yu Hongjian[c], Che Liyuan[a],Wang Ling[b] and Xiong Yan[b,*]

[a]School of Chemistry , Chemical engineering and Life science, Wuhan University of Technology, Wuhan, Hubei 430070, PR China

[b]School of Materials Science & Engineering, Hubei Province Key Laboratory of Green Materials for Light Industry, Hubei University of Technology, Wuhan, Hubei 430023, PR China

[c]State Key Lab of Advanced Technology for Materials Synthesis and Processing, Wuhan University of Technology, Wuhan, Hubei 430070, PR China

Peony-shaped grains of a $Ag_3PO_4/Zn_3(PO_4)_2$ composite has been synthesized at room temperature through coprecipitation and recrystallization technology with the coexistence of Zn^{2+} and Ag^+ in a aqueous solution.The simultaneous presence of high-concentration Ac^- ions plays a key role in the initial formation of flower-shaped grains of $Zn_3(PO_4)_2$ being the large- area host of this composite. Compared with pure Ag_3PO_4 crystals, the obtained composite exhibits enhanced visible-light-driven photocatalytic activity and stability for decomposition of Rhodamine B in aqueous solution. This is attributed to effective hole-electron pair transport and optimal Ag_3PO_4 dispersion achieved by confining Ag_3PO_4 to the as-prepared $Zn_3(PO_4)_2$ framework.

Keywords $Ag_3PO_4/Zn_3(PO_4)_2$ composite; ion exchange reaction; visible-light-driven photocatalytic activity

1 Introduction

In order to resolve environmental and energy issues, great efforts have been devoted for the removal of pollutants from water by developing more active visible-light-driven photocatalysts[1]. One such photocatalyst, Ag_3PO_4, has recently drawn attention due to its high efficiency in the photocatalytic degradation of dyes[2, 3]. It has been reported that Ag_3PO_4 crystals exhibit higher photocatalytic activity than N-doped TiO_2 on the degradation of methylene blue aqueous solution under visible light irradiation. In addition, Ag_3PO_4 crystals with high- energy crystal faces, porous Ag_3PO_4[4], and Ag_3PO_4-based heterostructured photocatalysts possess excellent performance for dyes degradation[5-9]. However, the stability of Ag_3PO_4 suffers from the dissolution of active

Ag^+-ions in the water and consequently results in the performance deterioration in repeated cycles[10]. Hence, effective methods should be explored to improve the stability of Ag_3PO_4 in photocatalysis process.

Immobilization of inorganic photocatalysts on inert supports has been attractive because it can help to stabilize the photocatalysts. Some suitable supports not only possess the ability of decreasing the recombination rate of electron-hole pairs but supplying a great amount of active sites. In addition, supports with excellent absorption performance can concentrate the pollutants from the solution to the photoactive sites of the photocatalysts. Different materials have been used as suitable supports for the photocatalysts, such as Al_2O_3[11], TiO_2[12], graphene[13], SBA-15[14] and C_3N_4[15]. Those supports can reduce the contact area of water with the catalysts and contribute to improving the stability of the target materials. The structural and morphological characteristics of the supports play important roles in the catalytic behavior. Therefore, choosing suitable supports is necessary for the enhancement of photocatalytic activity of Ag_3PO_4.

Flower-shaped inorganic semiconductor materials have been widely applied in the area of solar cell[16]and photocatalysis[17] due to their high specific surface area and effective hole-electron pair transport through the interconnected network. Template molecules containing strong coordinating groups have been used to mediate the formation of flower-like materials with large surface area. It is worth noting that flower-shaped Au[18], CdS[19], $Cu_3(PO_4)_2$[20, 21] and ZnO [22] crystal aggregates have been successfully synthesized with the participation of DNA, l-cysteine, BSA or ascorbate, respectively. However, the hybridization of inorganic materials with organic molecules would decrease the degree of crystallinity and material properties. Subsequent treatment of hybridized samples at temperature as high as 600-800°C is inevitable. Until now, there have been no reports of flower-shaped inorganic crystals made from pure inorganic components by means of facile synthetic routes in water.

For the first time, we report a novel method for creating peony-shaped grains of $Ag_3PO_4/Zn_3(PO_4)_2$ composite at room temperature in water without the addition of any organic molecules. The compound $Zn_3(PO_4)_2$ is a common host lattice for fluorescent materials like $Zn_3(PO_4)_2$:Hf [23], $Zn_3(PO_4)_2$:Eu [24] and $Zn_3(PO_4)_2$:Dy [25]. The environmentally friendly material will be applied in this study as the framework for Ag_3PO_4 crystals. In the preparation process,

large-area $Zn_3(PO_4)_2$ framework is firstly precipitated ruled by Ac^--ions and, secondly, Ag_3PO_4 is precipitated onto the surface of the $Zn_3(PO_4)_2$ support. Lastly, Ag_3PO_4 nanoparticles self-aggregate to form hierarchically flower-like structure, leading to the formation of well-distributed $Ag_3PO_4/Zn_3(PO_4)_2$ composite catalysts.

2. Results and discussion

2.1 Morphology and structure of the composites

The crystallinity and purity of the as-synthesized samples were investigated by XRD recordings. A XRD pattern of a typical $Ag_3PO_4/Zn_3(PO_4)_2$ composite is shown in Fig. 1a. The diffraction peaks denoted by "#" and "*" symbols are assigned to cubic Ag_3PO_4 (JCPDS 06-0505) and orthorhombic $Zn_3(PO_4)_2 \cdot 4H_2O$ (JCPDS 74−1778), respectively. SEM images of the corresponding sample are displayed at different magnifications in Fig. 1b-d. It illustrates that the typical morphology of the sample grains is a well-defined peony-shaped three-dimension structure with a diameter in the range of 4−8 μm. The peony-shaped grains are assembled by many densely arranged nano-thin sheet-shaped "petals". A close-up SEM view of this flower-like microstructure reveals that the sheets are about 100 nm in thickness, as seen in Fig.1d. The microscopic characteristic of flower-shaped composite was further analyzed by TEM (Fig.1S). TEM image verifies the microstructure of flower-like $Ag_3PO_4/Zn_3(PO_4)_2$ assembled with nano -thick plates (Fig.1Sa). Obvious contrast can be observed from the edge (Fig.1Sb). The microstructures indicate Ag_3PO_4 is covered by $Zn_3(PO_4)_2$ and the optimal Ag_3PO_4 dispersion is achieved by confining Ag_3PO_4 to the as-prepared $Zn_3(PO_4)_2$ framework.

.

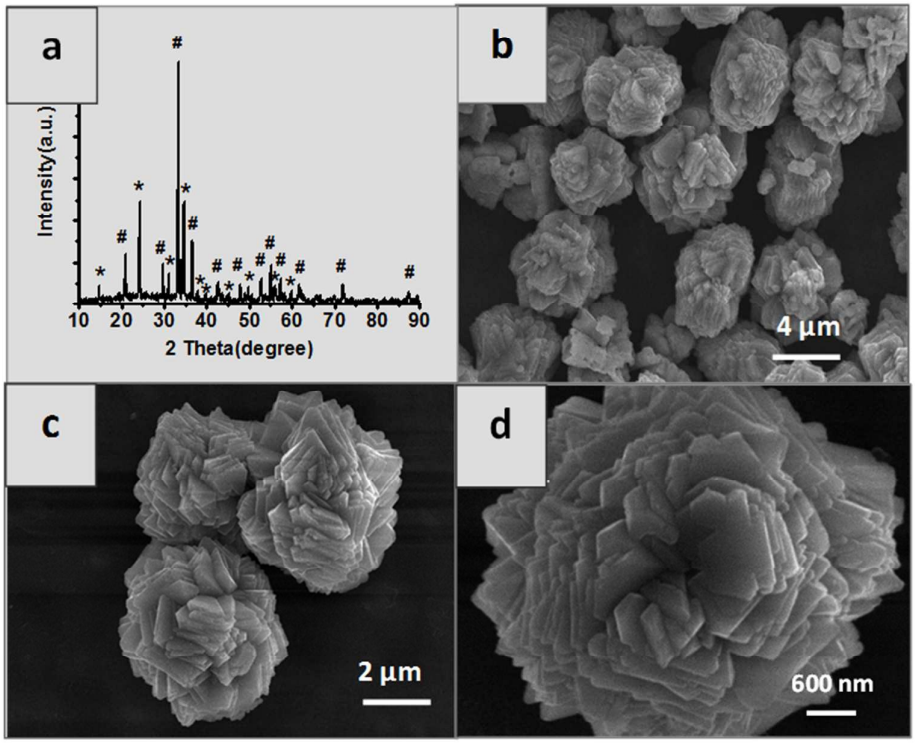

Fig.1 The XRD pattern and SEM images of a typical $Ag_3PO_4/Zn_3(PO_4)_2$ composite sample. (a) XRD pattern. The diffraction peaks denoted by "#" are assigned to cubic Ag_3PO_4 (JCPDS 06-0505). The other peaks denoted by signals of sea star are assigned to orthorhombic $Zn_3(PO_4)_2 \cdot 4H_2O$ (JCPDS 74−1778); (b)-(d) SEM images at different magnification.

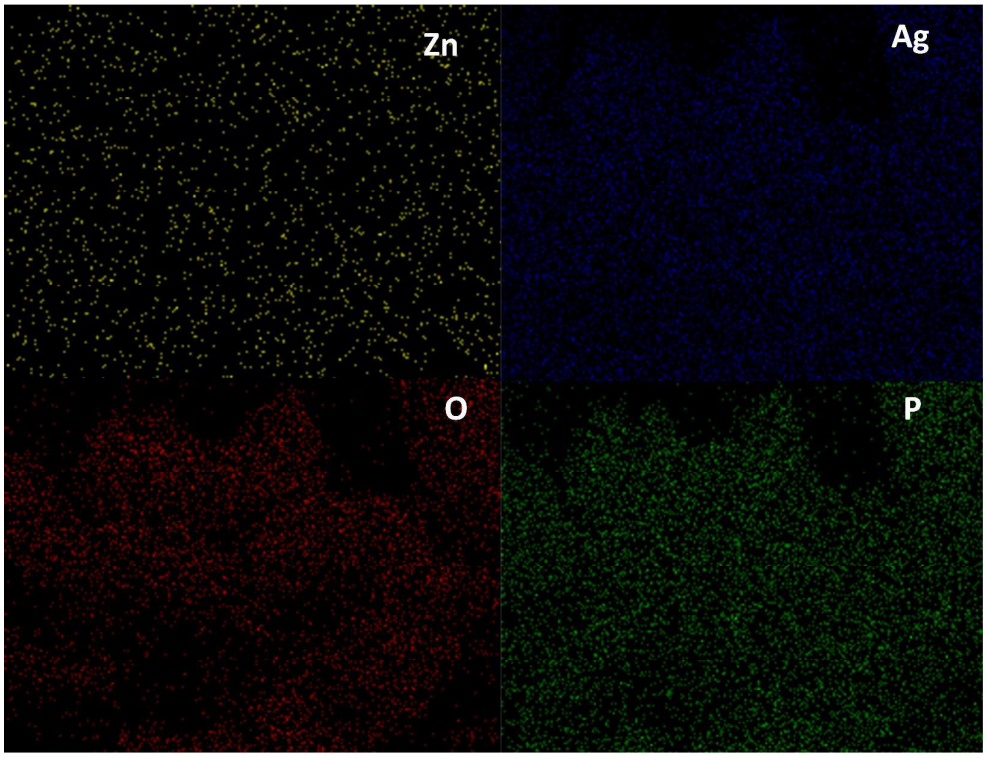

Fig. 2 Elemental maps of a flat surface of a flower from as-synthesized sample.

EDX analysis of the thin sheets forming the typical composite grains register the major elements Zn, Ag, O and P, as seen from Fig. 2S. The element signal of Al results from the sample support. The estimated atom ratio of Ag to Zn is 2.4. Elemental maps of the same sample clearly demonstrate uniform distribution of Zn, Ag, O and P elements over the flat surface, see Fig. 2. Hence, the typical sample is mainly composed of well-mixed Ag_3PO_4 and $Zn_3(PO_4)_2$ phases. The formation of a $Ag_3PO_4/Zn_3(PO_4)_2$ composite is further confirmed by measuring XPS spectra. The binding energy of Ag 3d5/2 and Ag 3d3/2 states corresponding to 368 and 374 eV peaks, respectively, are seen in Fig. 3a and are ascribed to the Ag-ion in Ag_3PO_4[26]. The binding energy of Zn $2p_{1/2}$ and Zn $2p_{2/3}$ located at 1045eV and 1022 eV, respectively, and seen in Fig. 3b are associated with Zn^{2+} in $Zn_3(PO_4)_2$[27].

2.2 Formation process of peony--shaped grains of the $Ag_3PO_4/Zn_3(PO_4)_2$ composite

XRD patterns of the $Ag_3PO_4/Zn_3(PO_4)_2$ composites prepared with different $AgNO_3$ concentration (at a fixed mole ratio of $Ag_3PO_4/Zn_3(PO_4)_2/KH_2PO_4$) are summarized in Fig. 4a. With the increase of $AgNO_3$ concentration, the diffraction peaks of Ag_3PO_4 become stronger，indicating the

crystalline degree of Ag_3PO_4 is improved gradually. The SEM morphology of $Ag_3PO_4/Zn_3(PO_4)_2$ composite grains prepared with 0.05M $AgNO_3$ solution is seen in Fig. 4b. The obtained sample consists of a large number of hierarchical crystals with an average size of 10-20 μm. The crystal agglomerates are assembled by octahedron-shaped crystals with a size of 4μm. For the sample prepared with 0.1M $AgNO_3$ solution, hierarchical crystal aggregates evolve into flower-like grains with a size of 5 μm and the building crystallites change from micro-sized octahedrons to thin plates, see Fig. 4c. Further increase of the $AgNO_3$ solution concentration (0.2 M) results in the formation of peony-shaped grain aggregates. These are assembled by nano-thick plates or "petals", as demonstrated earlier by SEM in Fig. 1b. The morphology of pure $Zn_3(PO_4)_2$ crystals as a reference consist of open and cross-linked interiors, see Fig. 4d. With the increase of reactant concentration, more $Zn_3(PO_4)_2$ and Ag_3PO_4 crystals are obtained resulting in that flower-shaped composite grains with more "petals". Increasing petals bring out more exposed crystal faces, which exhibit the superiority in the process of photocatalysis.

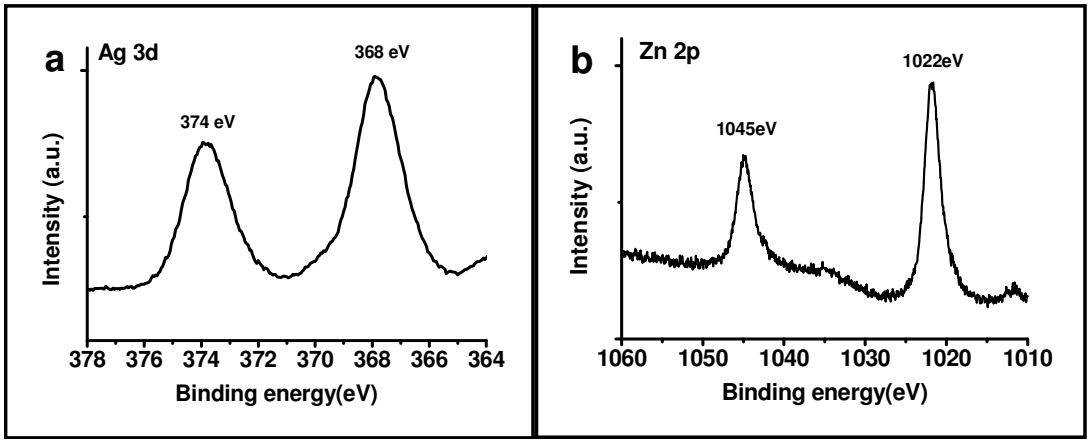

Fig. 3 XPS analysis of the as-synthesized sample, see text.

To further elucidate the formation process of peony-shaped $Ag_3PO_4/Zn_3(PO_4)_2$ crystal aggregates, the time dependent morphological evolution was examined by SEM. Corresponding XRD pattern and SEM images of the samples at different reaction periods are summarized in Fig.3S and Fig 5a-d. SEM images of the formed precipitates show that band-shaped AgAc (saturated solution) seen initially (2 min) changes to porous $Zn_3(PO_4)_2$ at a reaction time of 5 min, compare Fig. 4S and 5a. After 20 min, tiny Ag_3PO_4 nanoparticles appear on the surface of these porous $Zn_3(PO_4)_2$ grains (Fig.5b). When the reaction time is prolonged to 1.5h, more and larger Ag_3PO_4 crystals

grow and the flower-like structure is further pronounced (Fig. 5c). After 4-h reaction time the image of a peony-like composite grains around 4-8 μm are seen assembled by separated nano-sheets, see Fig. 5d. With a further extension of the reaction time, the morphology of the composite remains nearly unchanged, as shown earlier for 5 h in Fig.1d.

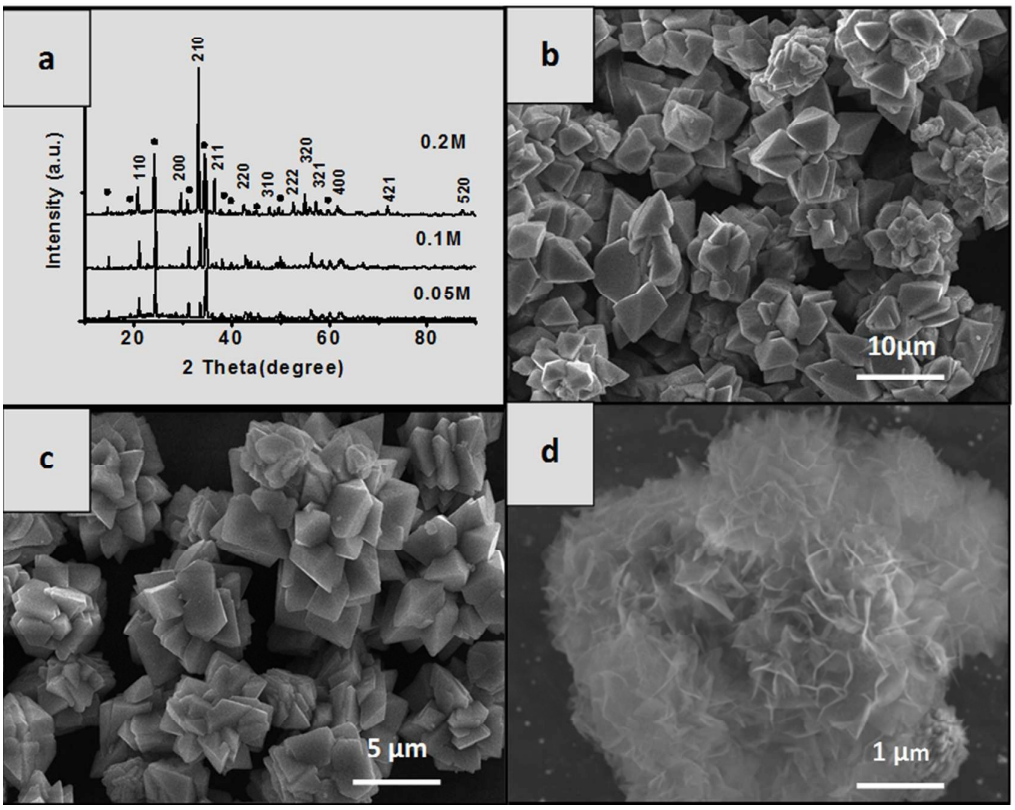

Fig.4 XRD patterns and SEM images of the samples prepared with different $AgNO_3$ concentration.(a) XRD patterns of $Ag_3PO_4/Zn_3(PO_4)_2$ composites prepared with different $AgNO_3$ concentration and a fixed mole ratio of $Ag_3PO_4/Zn_3(PO_4)_2$ /KH_2PO_4. The diffraction peaks denoted by "•" symbols are attributed to orthorhombic $Zn_3(PO_4)_2$•$4H_2O$ (JCPDS 74−1778) and the other diffraction peaks are attributed to cubic Ag_3PO_4 (JCPDS 06-0505). (b) and (c) Corresponding SEM images of $Ag_3PO_4/Zn_3(PO_4)_2$ composites prepared with 0.05M and 0.1M $AgNO_3$ solution. (d) SEM image of pure $Zn_3(PO_4)_2$ extracted from the solution before the formation of Ag_3PO_4.

To validate the function of Ac^- for the formation of peony-shaped $Ag_3PO_4/Zn_3(PO_4)_2$ composite grains, control experiments of two kinds of pure Ag_3PO_4 crystals were performed. Firstly, when

Ag_3PO_4 crystals are prepared by the direct reaction of 20 ml of 0.2M $AgNO_3$ and 20 ml of 0.1M KH_2PO_4 solution the Ag_3PO_4 crystals formed are composed of small particles with a size of 200-500 nm and some polyhedron particles with a size larger than 2 μm, as shown in Fig. 6a. Secondly, after replacing the $AgNO_3$ solution with an AgAc solution, micron-sized Ag_3PO_4 particles with several morphologies form, *e.g*. spherical, triangular pyramid or cubic as seen in Fig. 6b. These experiments indicate that flower-like Ag_3PO_4 could not create without $Zn_3(PO_4)_2$ framework. It is also shown that the morphology of $Zn_3(PO_4)_2$ grains extracted from the solution before the formation of Ag_3PO_4 are open and porous frame construction, see Fig. 4d. However, irregular sheet-shaped $Zn_3(PO_4)_2$ crystals with micro-scaled thickness are obtained by the direct reaction of $Zn(NO_3)_2$ solution (0.15M, 20 ml) and KH_2PO_4 solution (0.1M, 20 ml), as shown in Fig. 6c. It is clear that the open and porous $Zn_3(PO_4)_2$ crystals form in the presence of Ac^-. For further analysis, an $Ag_3PO_4/Zn_3(PO_4)_2$ composite was prepared with $Zn(NO_3)_2$ as Zn^{2+} source and with other experimental conditions unchanged. The obtained $Ag_3PO_4/Zn_3(PO_4)_2$ sample consists of a majority of tetrahedral particles with a size of 15 μm and a small quantity of cubic particles with a size of 5 μm, as seen in Fig. 6d. The observed morphology is obviously different from that of the $Ag_3PO_4/Zn_3(PO_4)_2$ composite obtained in the presence of Ac^-. Therefore, the interaction between Ac^- and Zn^{2+} on the surface of $Zn_3(PO_4)_2$ is the main driving force for forming porous $Zn_3(PO_4)_2$ framework. Secondary nucleation and growth of $Zn_3(PO_4)_2$ crystals originating at these Zn^{2+}-binding sites result in the formation of peony-shaped $Ag_3PO_4/ Zn_3(PO_4)_2$ composite grains with a large surface area.

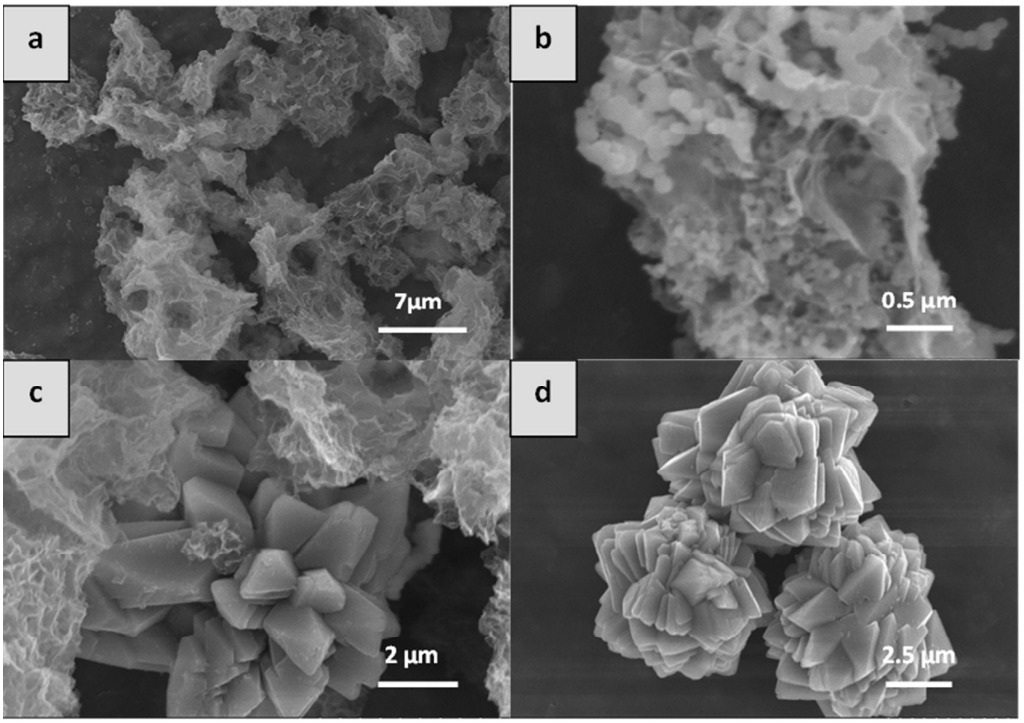

Fig. 5 SEM images of samples extracted from the solution for preparing peony-shaped $Ag_3PO_4/Zn_3(PO_4)_2$ composite at different reaction times. In (a) 5min; (b) 20min; (c)1.5 h; and (d) 4h.

In the reaction process, the following reactions (1) and (2) should be involved in the synthesis process of $Ag_3PO_4/Zn_3(PO_4)_2$ composite:

$$3Zn^{2+}(aq) + 2H_2PO_4^-(aq) = Zn_3(PO_4)_2(s) + 4H^+ \quad (1)$$

$$3Ag^+(aq) + H_2PO_4^-(aq) = Ag_3PO_4(s) + 2H^+ \quad (2)$$

$$6Ag^+(aq) + Zn_3(PO_4)_2(s) \leftrightharpoons 2Ag_3PO_4(s) + 3Zn^{2+}(aq) \quad (3)$$

Both Ag_3PO_4 and $Zn_3(PO_4)_2$ contain phosphate anions, therefore we should consider whether the transformation reaction occur from $Zn_3(PO_4)_2$ (A_3B_2 precipitate) to Ag_3PO_4 (A_3B_4 precipitate). The total equilibrium constant for the transformation reaction is calculated to be 0.459 according to the reaction (3) and the solubility product constants of Ag_3PO_4 (1.4×10^{-16}) and $Zn_3(PO_4)_2$ (9.0×10^{-33}), which means that the spontaneous trend at room temperature is small. A supplementary experiment was conducted to verify it. At room temperature, 20 ml of 0.15M

$Zn(NO_3)_2$ solution was mixed with 20 ml of 0.1M KH_2PO_4 solution to obtain pure $Zn_3(PO_4)_2$ precipitate, then 20 ml of 0.2M $AgNO_3$ solution was added . After reacting for 2h, the white precipitate did not change its color, which indicates that after $Zn_3(PO_4)_2$ crystallizes, it is difficult to transform to Ag_3PO_4 by ion-exchange process even in the Ag^+ saturated solution (see Fig.5S). It is believed that the formation of the peony-shaped Ag_3PO_4/ $Zn_3(PO_4)_2$ composite involves a coprecipitation process. In the reaction process, the color change of the precipitates can be observed from the photos taken at different time (Fig.6S). Slow release of Ag^+ from oversaturated AgAc decreases the formation speed of Ag_3PO_4, therefore Ag_3PO_4 precipitates appear after $Zn_3(PO_4)_2$ has precipitated completely.

On the basis of the above observations, the detailed formation process of peony-shaped $Ag_3PO_4/Zn_3(PO_4)_2$ composite undergoes three stages: (1) Oversaturated AgAc precipitates from the solution. (2) Ac^--ions induces the formation of an open $Zn_3(PO_4)_2$ skeleton. (3) The slow release of Ag^+ from supersaturated AgAc offers enough time for the initial formation of a $Zn_3(PO_4)_2$ skeleton .After that, Ag_3PO_4 nucleates on the surface of $Zn_3(PO_4)_2$ skeleton. Based on the above comparative experiments, we believe that the Ag_3PO_4 flowers involve a sequence of dissolution, recrystallization, and oriented attachment. With the presence of supersaturated AgAc, the tiny Ag_3PO_4 particles formed on the surface of $Zn_3(PO_4)_2$ skeleton undergo a crystal relocation process, which is a thermodynamic process. The larger Ag_3PO_4 particles continue to grow and become thinner depending on the dissolution of the smaller Ag_3PO_4 particles. The dissolved ions will initiate anisotropic regrowth of nano Ag_3PO_4 particles on the surface of the preexisted sheets to form peony-shaped structures. As the process continues and the solution keep supersaturated, nanosheets continue to grow until small Ag_3PO_4 particles disappear. Thereby the uniform flower-like composite were fabricated via a dissolution–recrystallization process, which is the driving force for the assembling of the hierarchical structure, such as flower-like α-$Ni(OH)_2$ microspheres[28] and anatase TiO_2[29], 3D- network polyaniline[30], porous ZnO-ZnSe nanocomposites[31], and porous $CoFe_2O_4$ microspheres[32].

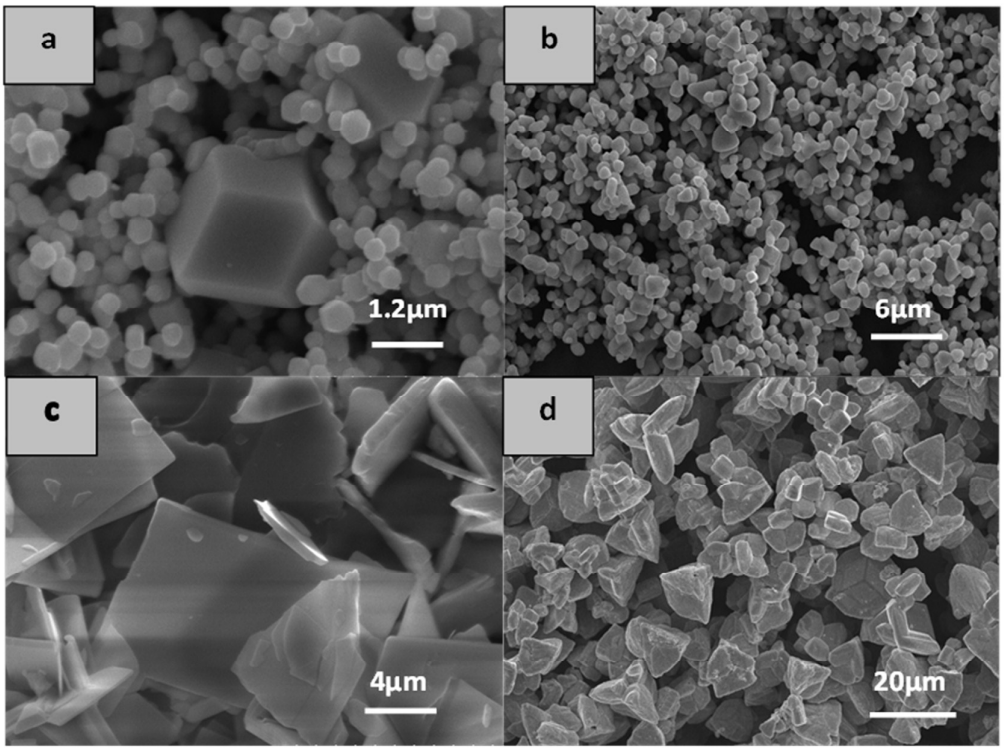

Fig. 6 SEM images of (a) pure Ag_3PO_4 crystals prepared with 0.2M $AgNO_3$ solution (20ml) and 0.1M KH_2PO_4 (20ml); (b) pure Ag_3PO_4 crystals prepared with 0.2M AgAc solution (20ml) and 0.1M KH_2PO_4 (20ml); (c) $Zn_3(PO_4)_2$ crystals prepared with same volume of 0.15M $Zn(NO_3)_2$ solution and 0.1M KH_2PO_4 solution; (d) $Ag_3PO_4/Zn_3(PO_4)_2$ composite prepared with 0.2M $AgNO_3$ solution (20ml), 0.15M $Zn(NO_3)_2$ solution (20ml) and 0.1M KH_2PO_4 (20ml).

2.3 Photocatalytic activity

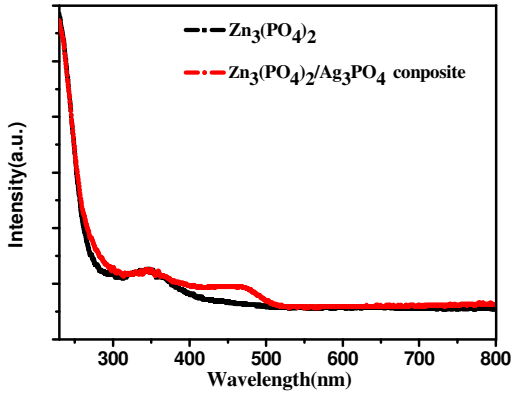

Fig. 7 UV-Vis diffusive absorption spectra of porous $Zn_3(PO_4)_2$ support and as-prepared

peony-shaped grains of the $Ag_3PO_4/Zn_3(PO_4)_2$ composite.

The UV-vis diffusive absorption spectra of as-prepared peony-shaped $Ag_3PO_4/Zn_3(PO_4)_2$ composite grains and the $Zn_3(PO_4)_2$ support are shown in Fig. 7. Both display an absorption in the region ranging from 250 to 400 nm, corresponding to the absorption of $Zn_3(PO_4)_2$[33]. Besides the absorption in the UV region, the $Ag_3PO_4/Zn_3(PO_4)_2$ composite can also absorb visible light with a wavelength range from 420 to 530 nm, which corresponds to the absorption range of pure Ag_3PO_4 (Fig. 7Sa). Thus, valence electrons of Ag_3PO_4 confined in the framework of $Zn_3(PO_4)_2$ can still be excited to the conduction band state by absorbing visible light, which suggests that the $Ag_3PO_4/Zn_3(PO_4)_2$ composite could be used as visible light photocatalysts. Fig. 7Sb indicates the bandgap of $Zn_3(PO_4)_2$ is 4.5eV based on the $(\alpha hv)^2$-hv curve.

Photoluminescence (PL) spectra of pure $Zn_3(PO_4)_2$, pure Ag_3PO_4 and peony-shaped $Ag_3PO_4/Zn_3(PO_4)_2$ composite were compared to inquire into the migration and separation efficiency of the photo-generated electrons and holes , as well as the surface vacancies. The emission peaks of $Zn_3(PO_4)_2$ and flower-like $Ag_3PO_4/Zn_3(PO_4)_2$ composite show similar characteristic (Fig.8Sa). For $Ag_3PO_4/Zn_3(PO_4)_2$ composite , the intensity of the peaks is weaker probably due to the covering of defect sites by Ag_3PO_4. For pure Ag_3PO_4, the broad PL peak centered at 557 nm is originated from the recombination of photoexcited electrons with holes [34](Fig.8Sb). The PL peak of Ag_3PO_4 disappears after the presence of $Zn_3(PO_4)_2$, which indicates that the combination of photogenerated electrons and holes occurred over Ag_3PO_4 is inhibited.

The photodegradation of RhB aqueous solution in the presence of peony-shaped grains of $Ag_3PO_4/Zn_3(PO_4)_2$ composite under visible light illumination is shown in Fig. 8a. The absorption peak of RhB at 554 nm decreases gradually and disappears in less than 60 min, suggesting a complete cleavage of RhB chromophores. Furthermore, the photodegradation curves of RhB in the form of C/C_0 as a function of irradiation time are utilized to compare the photocatalytic performance of $Ag_3PO_4/Zn_3(PO_4)_2$ with that of pure Ag_3PO_4, as shown in Fig. 8b. The photocatalytic reaction rate of $Ag_3PO_4/Zn_3(PO_4)_2$ is faster than that of pure Ag_3PO_4. The complete degradation of RhB dye over pure Ag_3PO_4 crystals takes about 170 min. Close to 100% of the dyes is removed over the $Ag_3PO_4/Zn_3(PO_4)_2$ composite within 60 min, whereas only 50%

of the dyes are degraded for pure Ag_3PO_4 catalyst during the same time duration.

To study the stability of the photocatalyst, $Ag_3PO_4/Zn_3(PO_4)_2$ composite grains used in above degradation process was collected and reused for additional RhB degradation cycles. After another 4 cycles of photodegradation of RhB solution under same visible light exposure time, the photocatalytic activity of $Ag_3PO_4/Zn_3(PO_4)_2$ composite shows a slight loss, see Fig. 8c. Therefore, the composite catalyst could be used more than 200 min, which exceeds the stability of pure Ag_3PO_4[35].

In order to explore the essential reasons for the enhanced performance produced by $Zn_3(PO_4)_2$ framework for Ag_3PO_4, active species trapping experiments were carried out. Three substances, including Isopropanol, benzoquinone (BZQ), and EDTA-2Na, were added at the beginning of the catalytic process as the scavengers of •OH, $•O_2^-$ and h^+, respectively. Fig.9S shows the photocatalytic curves of RhB solution over peony- shaped $Ag_3PO_4/Zn_3(PO_4)_2$ with the presence of different quenchers. The results show that the degradation trend of RhB has been completely inhibited by the addition of BZQ. While about 20 percent of degradation efficiency was lost after Isopropanol and EDTA-2Na were added, respectively. Consequently, $•O_2^-$, •OH and h^+ involve in the process of degrading dyes. Based on the previous report, the oxidization of RhB dyes over Ag_3PO_4 mainly depends on the h^+. Two reactions will occur after the formation of photogenerated electrons. O_2 molecules trap the electrons to produce $•O_2^-$ and photoreduction reaction ($Ag^+ + e^- \rightarrow Ag$) also consumes photogenerated electrons. For common Ag_3PO_4-based materials, the second reaction dominates, resulting in the failure of producing $•O_2^-$ radicals. For the peony-shaped $Ag_3PO_4/Zn_3(PO_4)_2$, the effective combination of Ag_3PO_4 with $Zn_3(PO_4)_2$ by the coprecipitation technology separates the electrons from the Ag^+, leading to the occurrence of $•O_2^-$-related reaction. On the other hand, with the assistance of $Zn_3(PO_4)_2$,partial holes on the surface of Ag_3PO_4 react with OH^- to produce •OH species, which has a strong oxidizing ability to decompose organic chemicals.

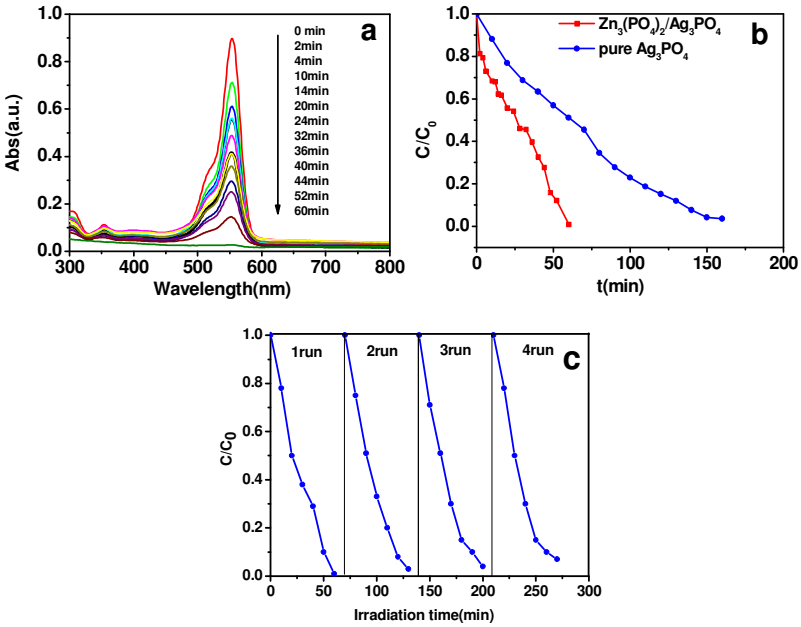

Fig. 8 (a) The photodegradation of RhB aqueous solution in the presence of peony-shaped grains of Ag_3PO_4/ $Zn_3(PO_4)_2$ composite under visible light illumination. (b) The photodegradation curves of RhB in the form of C/C_0 as a function of irradiation time. (c) Cycling runs in the photodegradation of RhB in the presence of used Ag_3PO_4/ $Zn_3(PO_4)_2$ composite under visible-light irradiation, *cf*. text.

The analysis of band structure of $Zn_3(PO_4)_2$ and Ag_3PO_4 are illustrated in Fig.9. The E_{CB} and E_{VB} of $Zn_3(PO_4)_2$ are calculated to be 0.59 and 5.09eV, respectively (The calculation was described in Support Information), therefore $Zn_3(PO_4)_2$ can accept the photogenerated electrons from Ag_3PO_4.

According to the detailed investigation, three factors are accounted for the excellent performance of peony- shaped $Ag_3PO_4/Zn_3(PO_4)_2$. Firstly, the specific surface area of peony-shaped $Ag_3PO_4/Zn_3(PO_4)_2$ is 28.20 $m^2\ g^{-1}$, which is higher than that of pure Ag_3PO_4 (13.71 $m^2\ g^{-1}$) and helps to increase the photocatalytic reaction sites. Secondly, three active species with high oxidizing ability, concluding $\bullet O_2^-$, •OH and h^+ , involve in the process of degrading dyes. Lastly, photogenerated electrons can transferred from the conduction band of Ag_3PO_4 to that of $Zn_3(PO_4)_2$. The special microstructure regulated by $Zn_3(PO_4)_2$ promotes the quick migration of

carriers, leading to the improvement of the separation efficiency of photo-generated electrons and holes.

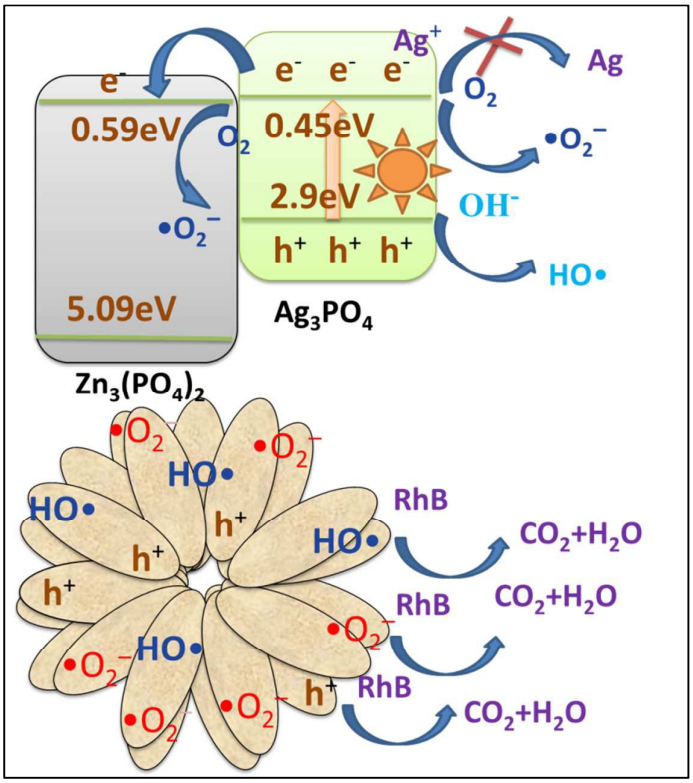

Fig.9. Schematic diagram of the photodegradation mechanism of peony- shaped $Zn_3(PO_4)_2$ / Ag_3PO_4 under visible light.

3 Experimental

3.1 Materials

All the reagents utilized in the present work were of analytical grade and were used without further purification.

3.2 Synthesis

The preparation procedure takes place in water solution. 20 ml of 0.2M $AgNO_3$ was added drop-wise to 20 ml of 0.15M $Zn(Ac)_2$ at room temperature. The obtained mixture (containing supersaturated AgAc) was stirred for 1h. Thereafter 20 ml of 0.1M KH_2PO_4 solution was added and a great amount of white precipitate formed immediately. The color of the precipitate changed

slowly from white to yellow during prolonged reaction time for 3h. Afterwards, the solution was transferred to a closed steel autoclave and heated at 110℃ for 2h. Subsequently, the precipitate was collected by centrifugation, thoroughly rinsed with distilled water and absolute ethanol before drying at 60℃ for 6 h. As a reference pure Ag_3PO_4 crystals were prepared in a similar way by mixing 20 ml of 0.1M KH_2PO_4 with 20 ml of 0.2M AgAc.

For exploring the formation of the obtained peony-shaped $Ag_3PO_4/Zn_3(PO_4)_2$ composite grains different $AgNO_3$ concentrations were used (0, 0.05, 0.1 and 0.2M) while keeping the same mole ratio of $AgNO_3$, $Zn(Ac)_2$ and KH_2PO_4.

3.3 Characterization

Powder X-ray diffraction (XRD) was carried out with a Rigaku D/max-2400 powder X-ray diffractometer. The morphologies of the as-synthesized samples were observed using JSM-5610LV scanning electron microscope (SEM) and Hitachi H-800 transmission electron microscope (TEM). X-ray photoelectron spectroscopy (XPS) was performed using an ESCALABMK II X-ray photoelectron spectrometer. UV-Vis diffusive absorption spectra were recorded on a Shimadzu UV2550 spectrophotometer. PL study was carried out on an Opticon 2 Luminescence Spectrometer with the excitation wavelength at 325 nm.

3.4 Photocatalytic experiments

The photocatalytic activity was investigated through the decomposition of a Rhodamine B (RhB) aqueous solution at room temperature. The reaction system, containing 100 ml of RhB solution with an initial concentration of 10^{-5} M and 50 mg of the tested photocatalysts, were placed in a cylindrical quartz vessel to record the absorption spectrum. Prior to irradiation, the reaction system was magnetically stirred in darkness for 0.5h to reach equilibrium. A visible light irradiation ($\lambda > 400$nm) through the quartz vessel was provided by a 150W Xe-lamp with UV-light filter. A sequence of UV-Vis spectra were collected at fixed time intervals to measure the RhB degradation by time.

4 Conclusions

In this paper, we present the first report on coprecipitation and recrystallization technology for

the fabrication of peony-shaped $Ag_3PO_4/Zn_3(PO_4)_2$ composite grains. The Ac^- ion is the key factor for ruling the initial precipitation of peony-shaped grains as it induce the formation of an open $Zn_3(PO_4)_2$ support. The support also reacts with excess of free Ag^+-ions in water from AgAc precipitate that slows the formation rate of Ag_3PO_4, leading to the formation of well-distributed Ag_3PO_4 upon the framework surfaces of the host. Compared with pure Ag_3PO_4 crystals, the obtained $Ag_3PO_4/Zn_3(PO_4)_2$ composite exhibits excellent visible-light-driven photocatalytic activity for the decomposition of RhB aqueous solution. This work illustrates a new way for fabrication of Ag_3PO_4 containing composites from pure inorganic components and promotes the practical applications of this catalyst in addressing environmental and energy issues.

Acknowledgements

This work was financially supported by National Natural Science Foundation of China (No. 51402097) , Natural Science Foundation of Hubei Province of China (112-45111811) and Fundamental Research Funds for the Central Universities (WUT: 2015IB002).

The authors are grateful to Prof. Thommy Eirkssion for his careful work on revising and polishing this paper.

References

1. Y. S. Xu and W. D. Zhang, *Dalton Trans*, 2013, **42**, 1094-1101.
2. Z. G. Yi, J. H. Ye, N. Kikugawa, T. Kako, S. X. Ouyang, H. Stuart-Williams, H. Yang, J. Y. Cao, W. J. Luo, Z. S. Li, Y. Liu and R. L. Withers, *Nature materials*, 2010, **9**, 559-564.
3. Y. Bi, S. Ouyang, N. Umezawa, J. Cao and J. Ye, *J Am Chem Soc*, 2011, **133**, 6490-6492.
4. Q. H. Liang, W. J. Ma, Y. Shi, Z. Li and X. M. Yang, *Crystengcomm*, 2012, **14**, 2966-2973.
5. Y. P. Bi, H. Y. Hu, S. X. Ouyang, Z. B. Jiao, G. X. Lu and J. H. Ye, *J Mater Chem*, 2012, **22**, 14847-14850.
6. X. F. Yang, H. Y. Cui, Y. Li, J. L. Qin, R. X. Zhang and H. Tang, *Acs Catal*, 2013, **3**, 363-369.
7. S. Kumar, T. Surendar, A. Baruah and V. Shanker, *Journal of Materials Chemistry A*, 2013, **1**, 5333-5340.
8. Z. M. Yang, G. F. Huang, W. Q. Huang, J. M. Wei, X. G. Yan, Y. Y. Liu, C. Jiao, Z. Wan and A. L. Pan, *Journal of Materials Chemistry A*, 2014, **2**, 1750-1756.
9. H. C. Yu, Q. S. Dong, Z. B. Jiao, T. Wang, J. T. Ma, G. X. Lu and Y. P. Bi, *Journal of Materials Chemistry A*, 2014, **2**, 1668-1671.
10. W. G. Wang, B. Cheng, J. G. Yu, G. Liu and W. H. Fan, *Chem-Asian J*, 2012, **7**, 1902-1908.
11. M. Bouslama, M. C. Amamra, Z. Jia, M. Ben Amar, K. Chhor, O. Brinza, M. Abderrabba, J. L.

Vignes and A. Kanaev, *Acs Catal*, 2012, **2**, 1884-1892.
12. L. X. Yang, S. L. Luo, Y. Li, Y. Xiao, Q. Kang and Q. Y. Cai, *Environmental science & technology*, 2010, **44**, 7641-7646.
13. Y. H. Zhang, Z. R. Tang, X. Z. Fu and Y. J. Xu, *Acs Nano*, 2010, **4**, 7303-7314.
14. J. Ma, J. Chu, L. S. Qiang and J. Q. Xue, *Rsc Adv*, 2012, **2**, 3753-3758.
15. S. Kumar, S. Tonda, A. Baruah, B. Kumar and V. Shanker, *Dalton T*, 2014, **43**, 16105-16114.
16. J. X. Wang, C. M. L. Wu, W. S. Cheung, L. B. Luo, Z. B. He, G. D. Yuan, W. J. Zhang, C. S. Lee and S. T. Lee, *J Phys Chem C*, 2010, **114**, 13157-13161.
17. M. Ge, J. W. Li, L. Liu and Z. Zhou, *Ind Eng Chem Res*, 2011, **50**, 6681-6687.
18. Z. D. Wang, J. Q. Zhang, J. M. Ekman, P. J. A. Kenis and Y. Lu, *Nano Lett*, 2010, **10**, 1886-1891.
19. S. L. Xiong, B. J. Xi and Y. T. Qian, *J Phys Chem C*, 2010, **114**, 14029-14035.
20. Y. Huang, X. Ran, Y. Lin, J. Ren and X. Qu, *Chem Commun (Camb)*, 2015, **51**, 4386-4389.
21. J. Sun, J. Ge, W. Liu, M. Lan, H. Zhang, P. Wang, Y. Wang and Z. Niu, *Nanoscale*, 2014, **6**, 255-262.
22. M. Raula, M. H. Rashid, T. K. Paira, E. Dinda and T. K. Mandal, *Langmuir*, 2010, **26**, 8769-8782.
23. Z. Peng, Z. Xu, C. Luo, J. Yu and G. Zhang, *Luminescence : the journal of biological and chemical luminescence*, 2008, **23**, 14-16.
24. X. Z. Xiao, B. Yan and Y. S. Song, *Cryst Growth Des*, 2009, **9**, 136-144.
25. N. Vijaya, K. Upendra Kumar and C. K. Jayasankar, *Spectrochimica acta. Part A, Molecular and biomolecular spectroscopy*, 2013, **113**, 145-153.
26. Y. He, L. Zhang, B. Teng and M. Fan, *Environmental science & technology*, 2015, **49**, 649-656.
27. M. J. Dinsmore and J. S. Lee, *Journal of inorganic biochemistry*, 2008, **102**, 1599-1606.
28. H. Du, L. Jiao, K. Cao, Y. Wang and H. Yuan, *ACS Appl Mater Interfaces*, 2013, **5**, 6643-6648.
29. J. Yu, Y. L. Yang, R. Q. Fan, L. Li and X. Y. Li, *J Phys Chem C*, 2014, **118**, 8795-8802.
30. W. Ding, L. Li, K. Xiong, Y. Wang, W. Li, Y. Nie, S. Chen, X. Qi and Z. Wei, *J Am Chem Soc*, 2015, DOI: 10.1021/jacs.5b00292.
31. S. Cho, J. W. Jang, J. S. Lee and K. H. Lee, *Nanoscale*, 2012, **4**, 2066-2071.
32. B. Cai, M. Zhao, Y. Ma, Z. Ye and J. Huang, *ACS Appl Mater Interfaces*, 2015, **7**, 1327-1333.
33. N. Xie, D. C. Feng, H. Li, C. W. Gong and L. Zhen, *Mater Lett*, 2012, **82**, 26-28.
34. Q. H. Liang, Y. Shi, W. J. Ma, Z. Li and X. M. Yang, *Phys Chem Chem Phys*, 2012, **14**, 15657-15665.
35. P. Ma, A. Chen, Y. Wu, Z. Fu, W. Kong, L. Che and R. Ma, *J Colloid Interface Sci*, 2014, **417**, 293-300.